



HAL
open science

Evidence of Non-thermal Hydrogen in the Exosphere of Mars Resulting in Enhanced Water Loss

Dolon Bhattacharyya, J. T. Clarke, M. Mayyasi, V. Shematovich, D. Bisikalo, Jean-Yves Chaufray, E. Thiemann, J. Halekas, C. Schmidt, Jean-Loup Bertaux, et al.

► **To cite this version:**

Dolon Bhattacharyya, J. T. Clarke, M. Mayyasi, V. Shematovich, D. Bisikalo, et al.. Evidence of Non-thermal Hydrogen in the Exosphere of Mars Resulting in Enhanced Water Loss. *Journal of Geophysical Research. Planets*, 2023, 128 (8), pp.e2023JE007801. 10.1029/2023JE007801 . insu-04178450

HAL Id: insu-04178450

<https://insu.hal.science/insu-04178450>

Submitted on 8 Dec 2023

HAL is a multi-disciplinary open access archive for the deposit and dissemination of scientific research documents, whether they are published or not. The documents may come from teaching and research institutions in France or abroad, or from public or private research centers.

L'archive ouverte pluridisciplinaire **HAL**, est destinée au dépôt et à la diffusion de documents scientifiques de niveau recherche, publiés ou non, émanant des établissements d'enseignement et de recherche français ou étrangers, des laboratoires publics ou privés.

Copyright

Key Points:

- Observations of H brightness at high altitude in Mars' atmosphere during aphelion solar minimum show an abrupt slope change above 5,000 km
- Hot H atoms produced via solar wind charge exchange can reproduce the observed profiles, providing evidence for nonthermal hydrogen
- Since this escape scales with solar wind flux, elevated loss rates early in Mars' history could result in much larger overall water loss

Correspondence to:

D. Bhattacharyya,
dolon.bhattacharyya@lasp.colorado.edu

Citation:












Bhattacharyya, D., Clarke, J. T., Mayyasi, M., Shematovich, V., Bisikalo, D., Chaufray, J. Y., et al. (2023). Evidence of non-thermal hydrogen in the exosphere of Mars resulting in enhanced water loss. *Journal of Geophysical Research: Planets*, 128, e2023JE007801. <https://doi.org/10.1029/2023JE007801>

Received 27 FEB 2023
Accepted 30 JUL 2023

Author Contributions:

Conceptualization: D. Bhattacharyya, J. T. Clarke
Data curation: D. Bhattacharyya
Formal analysis: D. Bhattacharyya, M. Mayyasi
Funding acquisition: D. Bhattacharyya, J. T. Clarke, N. M. Schneider
Investigation: D. Bhattacharyya, M. Mayyasi, E. Thiemann, J. Halekas
Methodology: D. Bhattacharyya, C. Schmidt, J. L. Bertaux, M. S. Chaffin
Project Administration: J. T. Clarke
Software: D. Bhattacharyya, V. Shematovich, D. Bisikalo, J. Y. Chaufray
Supervision: J. T. Clarke
Writing – original draft: D. Bhattacharyya
Writing – review & editing: J. T. Clarke, M. Mayyasi, V. Shematovich, D. Bisikalo, J. Y. Chaufray, E. Thiemann, J. Halekas, C. Schmidt, J. L. Bertaux, M. S. Chaffin, N. M. Schneider

Evidence of Non-Thermal Hydrogen in the Exosphere of Mars Resulting in Enhanced Water Loss

D. Bhattacharyya¹ , J. T. Clarke² , M. Mayyasi² , V. Shematovich³, D. Bisikalo³ , J. Y. Chaufray⁴ , E. Thiemann¹ , J. Halekas⁵ , C. Schmidt² , J. L. Bertaux⁴ , M. S. Chaffin¹ , and N. M. Schneider¹ 

¹Laboratory of Atmospheric and Space Physics, University of Colorado Boulder, Boulder, CO, USA, ²Center for Space Physics, Boston University, Boston, MA, USA, ³Institute of Astronomy, Russian Academy of Sciences, Moscow, Russia, ⁴Laboratoire Atmosphères, Milieux, Observations Spatiales (LATMOS), Guyancourt, France, ⁵Department of Physics and Astronomy, University of Iowa, Iowa City, IA, USA

Abstract Atomic H is a direct tracer of water loss at Mars. The recent discovery of annual enhancements in its escape rate near perihelion, in excess of the previously established theory, indicates that Mars has lost substantial amounts of water to space. However, these loss rates are often estimated assuming thermal properties for the exospheric H atoms and are therefore a lower limit. Past analyses of spacecraft observations delivered indirect evidence for the existence of an energetic non-thermal H population without a clear detection. Here, we present the unambiguous observational signature of non-thermal H at Mars, consistent with solar wind charge exchange as the primary driver for its production. The calculated non-thermal escape rates are as high as ~26% of the thermal rate near aphelion and solar minima. An active Sun would increase the present-day escape rate and a younger energetic Sun likely contributed toward the significant historic loss of water from Mars.

Plain Language Summary The total water lost by Mars is determined by calculating the number of H atoms permanently escaping its upper atmosphere into space at present and extrapolating it back in time. The present-day escape rate of H does not account for energetic H atoms, which were postulated to exist but not previously observed to date. Such a population would enhance the H escape rate further, thereby increasing the total volume of the water lost by Mars. This work presents the first confirmed signature of energetic H atoms in the atmosphere of Mars and finds that interaction of the neutral H population in its uppermost atmospheric layer, that is, its exosphere, with the solar wind results in its creation. The amount of energetic H atoms produced depends on the Mars' atmospheric conditions such as temperature and density of neutral H atoms in the exosphere, solar activity, and Mars' position around the Sun. Since the younger Sun was much more active than today, it is likely that the interaction of an early Martian exosphere with the stronger solar wind resulted in the loss of a larger fraction of H atoms into space than has been estimated to date.

1. Introduction

Water loss from Mars has been the subject of intense scrutiny in the past few decades. Surface geological features stipulate that Mars was host to large lakes and streams early in its evolutionary history (Baker, 2001; Ehlmann et al., 2011; Jakosky & Philips, 2001; Ojha et al., 2015). Today's Mars is dry and barren. Loss of its global magnetic field and its once thick CO₂ atmosphere facilitated the slow escape of the planet's water inventory into space, to some extent, over a timeframe of several billion years (Jakosky et al., 2018). At present though, accurate knowledge of the water reserves once possessed by Mars and the percentage lost to space is lacking. Estimates from mapping the D/H ratio of near-surface water quote a global equivalent layer (GEL) of ~140 m hosted by nascent Mars, whereas remote sensing measurements of its exosphere advocate a GEL of ~23 m (Jakosky et al., 2018; Villanueva et al., 2015). The GEL describes the thickness a certain volume of water would have if it were spread evenly over all of Mars's surface. This large discrepancy between the surface and remote sensing estimates is due in part to factors that are unaccounted for in the remote sensing analyses. One of them is the assumption that the hydrogen atoms at Mars, the primary source of which is photodissociated water vapor, are only undergoing escape from its exosphere based on the velocity distribution at the inferred bulk gas temperature, that is, thermal escape.

The highly expansive Martian exosphere was first discovered by the Mariner 6 and 7 probes in the late 1960s and early 1970s through the detection of the resonantly scattered solar Lyman α photons by its H atoms at

altitudes of $\sim 8.8 R_{\text{Mars}}$ (Barth et al., 1969, 1971). Since then, martian exospheric characterization has made remarkable headway using the same remote sensing technique. Analysis of the Lyman α emission line observed with far-ultraviolet imaging using the Hubble Space Telescope (HST) and Mars Express (MEX) determined an order of magnitude change in the thermal H escape flux during the southern summer season (Bhattacharyya et al., 2015; Chaffin et al., 2014; Clarke et al., 2014), with the peak escape occurring around Southern Summer Solstice, that is, when the south pole is at its highest sunward tilt (Bhattacharyya et al., 2017b). This trend was also identified by the Mars Atmosphere and Volatile Evolution (MAVEN) mission, which furthered the timeline of the observations over multiple Mars Years and confirmed a similar behavior for the deuterium atoms (Clarke et al., 2017; Halekas, 2017; Mayyasi et al., 2019, 2022). Despite all these discoveries, none could establish unambiguous evidence for the presence of energetic non-thermal H atoms in the exosphere of Mars.

Non-thermal H atoms are atoms created via non-thermal processes with velocity distributions that do not obey the standard Maxwell-Boltzmann profile. These atoms may have higher energies compared to thermal H in planetary exospheres and are therefore often referred to as hot atoms. Various processes may give rise to non-thermal H in planetary exospheres, the most influential among those being exothermic/photochemical reactions with H bearing species close to the exobase (boundary between the collisional and collisionless atmosphere), collisions between other non-thermal species and thermal H atoms, and charge exchange between thermal H and incident solar wind protons. All these processes are active at Mars. However, little is known about the exact contribution of each process in the production of the Martian exospheric non-thermal H atoms as no direct detections of energetic H were made until this work.

The first indirect indicator of non-thermal H at Mars was inferred during the analysis of MEX observations of the Martian exospheric Lyman α emission (Chaffin et al., 2014; Chaufray et al., 2008). Well appropriated temperature boundaries (~ 170 – 350 K) for the thermal H atoms, determined from thermospheric observations and Global Circulation Models, could not reproduce the MEX Spectroscopy for the Investigation of the Atmosphere of Mars instrument's Lyman α intensity profiles (Bougher & Keating, 1999; Bougher et al., 2009; Leblanc et al., 2006, 2007). Instead, a substantially higher temperature (>350 K) was required to match the observed intensities. The same was true for the HST observations of Mars (Bhattacharyya et al., 2015, 2017a, 2017b; Clarke et al., 2014). Attempts at spectrally separating an energetic population from the dominant thermal H atoms did not yield any positive results as the temperature difference between the two was not large enough to be observed as perceivable Doppler broadening within the spectral resolution of the available instruments.

An alternate means toward isolating energetic non-thermal H is to discern a transformation in the slope of the Lyman α intensity profile as the mean atmospheric scale height, that is, the distance over which the atmospheric density falls by a factor of an exponent, transitions from being thermally dominated to becoming non-thermal H dominated at high altitudes. This is a well-known characteristic of the Lyman α profiles of Venus (Anderson, 1976; Bertaux et al., 1978; Chaufray et al., 2012). The density distribution of the thermal H atoms declines rapidly with altitude at Venus due to its substantial gravity in comparison to Mars. The larger scale height of the Martian exosphere due to the low gravity results in a more gradual decrease of the H density profile making it difficult to observe the transition altitude above which energetic non-thermal H becomes dominant.

To test for the presence of an extended non-thermal H corona at Mars, HST observations specifically tailored toward detecting this population were scheduled during the end of 2017 and beginning of 2018. This work presents those observations and their detailed analysis to positively identify the presence of non-thermal H atoms on Mars, characterize them, and determine their role in the water loss history of the planet.

2. HST Observations of Mars

The martian exospheric Lyman α emission was imaged using the Advanced Camera for Surveys—Solar Blind Channel (ACS-SBC) onboard the HST. The ACS-SBC instrument is a broadband imager optimized for the far ultraviolet wavelength range of 115–170 nm. The sensitivity of the ACS-SBC detector at Lyman α is well constrained through an independent HST observing campaign (Bhattacharyya et al., 2020).

The HST observations consisted of 300 s exposures of Mars with a clear filter which allows Lyman α and another that blocks it out. The scaled difference of the two images contains only the Lyman α emission above the limb of Mars. The disk, however, is too noisy to be used after the subtraction process because of FUV emissions from oxygen, and nitrogen which dominate the thermospheric altitudes at Mars. The density of the heavier species

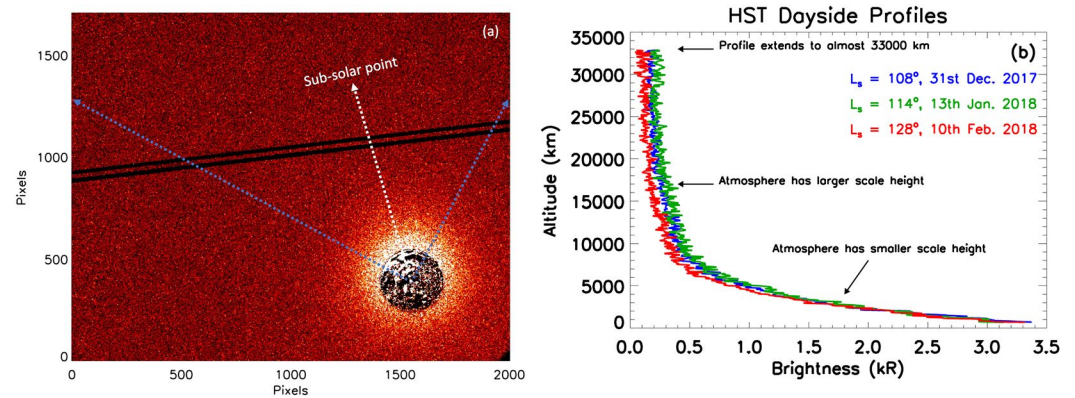


Figure 1. (a) The final reduced Advanced Camera for Surveys—Solar Blind Channel image of the martian Lyman α emission for 31 December 2017. The two parallel black lines are dead anodes on the detector. The disk of Mars is noisy as the difference between the clear and filtered image is very small. The blue lines mark the $\pm 45^\circ$ angle around the sub-solar point wherein pixels within the same angular distance from the disk center were averaged to obtain the Lyman α intensity profile with altitude at Mars. (b) The intensity profile with altitude constructed for the three Hubble Space Telescope visits ranging from $1 R_{\text{Mars}}$ (0 km) to $11.32 R_{\text{Mars}}$ (35,000 km).

falls off rapidly due to their smaller scale height, and above $\sim 1,000$ km the signal from H Lyman α is $>90\%$ of the total signal measured as H is the dominant species everywhere at and above that region (Krasnopolsky, 2010).

Lyman α emissions from background sources like the geocorona and the interplanetary hydrogen vary with HST's position in its orbit and its look direction. This background manifests itself as a constant value on top of the Mars Lyman α signal. The geocoronal intensity may vary from ~ 1 kR on the anti-sunward side to ~ 30 kR on the dayside depending on solar activity across HST's orbit (Bhattacharyya et al., 2020; Waldrop & Paxton, 2013). Therefore, to quantify this constant background a separate HST orbit observing the blank sky 5 arcminutes away from Mars was included as part of the observing campaign. Since each visit consisted of ~ 11 images of Mars with the clear filter, corresponding images from the sky orbit were used to estimate the background Lyman α intensity for each Mars image (values between 2 and -20 kR), which was then subtracted off from them. The final reduced image containing only the Martian exospheric Lyman α emission is shown in Figure 1a. The ACS-SBC image reduction procedure is detailed in Clarke et al. (2009).

Due to the large scale height of thermal H in the Martian exosphere, the HST observations were executed during low solar activity ($F_{10.7} < 80$ at Earth) and at orbital longitudes closest to Mars' aphelion ($L_s = 71^\circ$) given HST's scheduling constraints. These observing conditions ensured colder temperatures for the thermal H atoms and therefore a reduced scale height. The Earth-Mars distance was also greater than 1.5 AU, enabling the global imaging of the Martian exosphere up to altitudes of $\sim 33,000$ km. The observations were executed as three separate visits over a period of 2 months beginning on the last day of 2017. Table 1 details the exact observing conditions.

Radial intensity profiles, in kilo-Rayleighs (1 kilo-Rayleigh = 10^9 photons/cm²/s), were constructed by taking a $\pm 45^\circ$ angular slice around the sub-solar point in the final reduced images. This technique averages the pixel intensities equidistant from the planet's center to construct the altitude profile. Since the number of pixels increases with distance from planet center, this method allows for a better signal-to-noise ratio at higher altitudes where the photon count in each pixel is small.

The profile for each observation day displays an abrupt change in slope between 5,000–10,000 km, as shown in Figure 1b. At these altitudes, the mean scale height of the atmosphere starts transitioning from being thermal H dominated to non-thermal H dominated and is similar to the double sloped profiles observed at Venus (Chaufray et al., 2012). For plotting purposes, Figures 2a–2c show the mean of the three observations and their corresponding model fits, instead of the individual days, for better visibility of the profile shape at high altitudes. The analysis was done for each observation independently.

The ACS-SBC instrument is a photon counting Multi Anode Microchannel Array detector with very low dark current (8.52×10^{-6} counts/s/pix) and zero read noise. The quantum efficiency of the detector is $\sim 34\%$ at Lyman α (Ryon et al., 2023). Hence, the noise contribution from the detector itself is very small. The total uncertainty

Table 1
Hubble Space Telescope Observing Conditions and Thermal H Fit to the Data

Observation Date	Sun—Mars distance (AU)	Mars solar longitude (L_s) ($^\circ$)	Earth—Mars distance (AU)	$F_{10.7}$ index at Earth	Exobase temperature for thermal H at SZA = 0° (K)	^a Best-fit thermal H density at the exobase (cm^{-3})	^b Escape flux of thermal H from the exobase ($\times 10^7$ atoms/ cm^2/s)
12/31/2017 365	1.63	108	1.96	71	271	$42,700 \pm 2,300$	8.06 ± 0.43
01/13/2018 013	1.62	114	1.85	71	218	$68,600 \pm 8,200$	3.86 ± 0.46
02/10/2018 042	1.59	128	1.58	78	190	$83,600 \pm 5,400$	1.88 ± 0.12

^aUncertainties derived from $\chi^2_{\text{min}} + 1$ from the radiative transfer (RT) model thermal H fits to the HST data. ^bUncertainty calculated from the thermal H exobase density limits given in the seventh column.

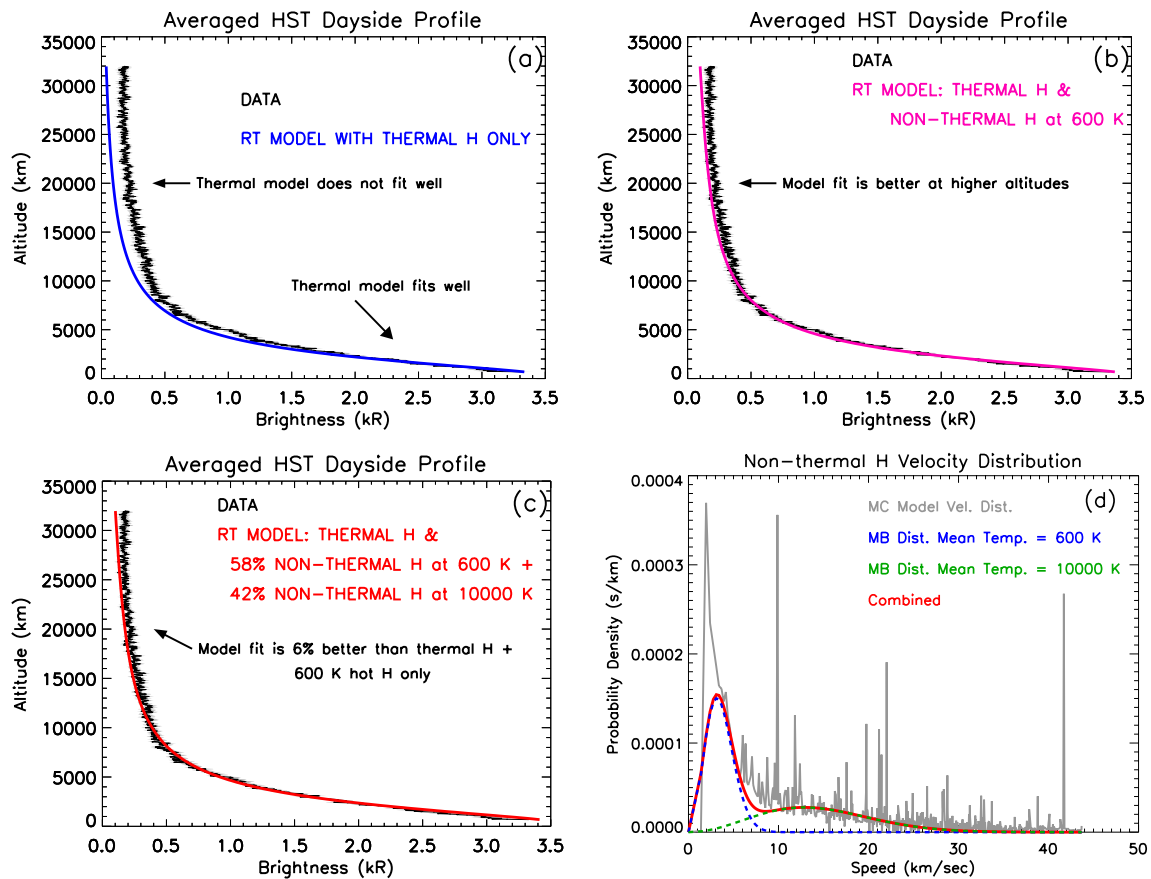


Figure 2. (a) The radiative transfer model best-fit to the Hubble Space Telescope (HST) data considering only thermal H atoms in the Martian exosphere. (b) The model fit to the data upon adding a non-thermal H population at a mean temperature of 600 K in the Martian exosphere to the thermal H intensity shown in panel (a). (c) An improved fit to the data by 6% at altitudes between 12,000–30,000 km upon including the high energy tail of the velocity distribution of H atoms with a 10,000 K Maxwellian. The uncertainty in the data values is $<30\%$ for the HST observations and is represented by the light gray shaded region in panels (a–d). The Maxwellian functional fits to the non-thermal H speed distribution obtained from the Monte Carlo (MC) model at an altitude of 240 km, which is close to the 200 km exobase altitude for Mars assumed in the thermal H model. The model curve (gray) is noisy because of the inherent randomness of the MC modeling process and the small number density of hot H atoms.

in the derived intensity values in the final altitude profiles is ~25%–30% for the highest altitudes (>20,000 km) with values <5% at the lower altitudes (<5,000 km). This uncertainty is represented as a gray-shaded region in Figures 2a–2c.

3. Modeling the Thermal H Distribution in the Exosphere of Mars

The density distribution of the H atoms corresponding to the observed intensity in the HST images are non-linearly related at altitudes below ~20,000 km. Here the Lyman α emission is optically thick, that is, the solar photons are resonantly scattered in random directions by multiple H atoms before reaching the observer. A RT model that accounts for the scattering probabilities is required to accurately estimate the line-of-sight Lyman α emission intensity. For this analysis, an existing RT model, previously used to study the martian Lyman α emission has been used to simulate the observed intensities (Bhattacharyya et al., 2015, 2017a, 2017b; Clarke et al., 2017). This model assumes spherical symmetry and an isothermal exosphere, which works well for the observed high altitudes with HST (Bhattacharyya et al., 2020). The model also assumes a Maxwellian velocity distribution for the H atoms at the exobase (thermal H atoms).

RT modeling of the optically thick Lyman α emission results in a degeneracy between its two free parameters, temperature and number density of the thermal H atoms at the exobase (Bhattacharyya et al., 2017a; Chaffin et al., 2018). This degeneracy is broken by independently determining the thermospheric temperature at Mars and assigning it to be the mean temperature of the thermal H atoms at the exobase, as has been done in previous studies (Bhattacharyya et al., 2015, 2017a, 2017b; Clarke et al., 2017; Mayyasi et al., 2018, 2019, 2022).

The majority of thermal H at Mars is created via photodissociation of water vapor over a range of altitudes (40–80 km). H as H₂ is then transported via both diffusion and bulk dynamics to the upper thermosphere and re-converted back into atomic H in ionospheric reactions (Hunten & McElroy, 1970; McElroy & Donahue, 1972; Parkinson & Hunten, 1972). Due to this, the H atoms are expected to be in thermal equilibrium with the thermosphere where the collision frequency with CO₂ is still large in comparison to the exobase altitude (~200 km). Therefore, the Martian thermospheric temperature is a close estimate of the thermal H mean temperature at the exobase.

For the first two HST observations, the thermospheric temperature was determined from MAVEN's Extreme UltraViolet Monitor (EUVM) occultation measurements near the terminator (Thiemann et al., 2018). This temperature was then converted to the sub-solar point value using the temperature versus solar zenith angle (SZA) curve established at Mars from MAVEN's Neutral Gas and Ion Mass Spectrometer (NGIMS) measurements (Bhattacharyya et al., 2020). Due to MAVEN's precessing orbit and its unfavorable observing geometry, the thermospheric temperature for the last HST observation could not be obtained from EUVM measurements. Instead, the Mars-Planetary Climate Model (Mars-PCM) was used to obtain the thermospheric temperature at the sub-solar point (Forget et al., 1999; Gonzalez-Galindo et al., 2009). The exobase temperature at Mars does not vary much with SZA < 60° on the dayside (Bhattacharyya et al., 2020; Mayyasi et al., 2022; Stone et al., 2018). Since the HST profiles are on the dayside around the subsolar point ($\pm 45^\circ$), the above-described temperatures are a good estimate for the exobase in the spherically symmetric RT model.

The density distribution of thermal H atoms that best matched the HST observations was determined using the RT model. Simulated Lyman α intensities for different thermal H exobase densities were fit to the data with the constraint that the modeled intensity cannot exceed the observed intensity up to an altitude of ~2,700 km, where >90% of the H atoms were assumed to be thermal. This constraint is to ensure that more weight is given toward fitting the simulated values of the “thermal H only” model to the observed intensities at altitudes <5,000 km, where most of the thermal H atoms reside. The best-fit density was determined through χ^2 minimization (Chaufray et al., 2008). The altitude of ~2,700 km was chosen as it was the highest altitude with the lowest χ^2 up to which the mean of the modeled intensity did not exceed the mean of the observed intensity for all the observations. Figure 2a displays the best-fit model intensity for thermal H plotted against the HST data. The uncertainties in the derived density were determined from the maximum and minimum bound of the range of densities encompassed by $\chi^2_{\min} + 1$ for the model fit. Table 1 lists the corresponding H exobase densities for the three HST observations. The thermal escape flux in Table 1, Φ_{Jeans} , is calculated using the Jeans formulation:

$$\Phi_{\text{Jeans}} = \frac{n(r_{\text{exo}}) e^{-\lambda_{\text{exo}}} U_{\text{th}}}{2\sqrt{\pi}} (\lambda_{\text{exo}} + 1) \quad (1)$$

In the above equation, U_{th} is the most probable Maxwellian velocity for the H atoms given by $U_{th} = \sqrt{\frac{2k_b T_{exo}}{m}}$, λ_{exo} is a dimensionless parameter given by, $\lambda_{exo} = \frac{v_{esc}^2}{U_{th}^2} = \frac{GMm}{k_b T_{exo} r_{exo}}$ with v_{esc} being the parabolic escape velocity for hydrogen, G as the universal gravitational constant, M the mass of Mars, k_b as the Boltzmann constant, T_{exo} as the temperature at the exobase, n the number density of H, and r_{exo} as the altitude of the exobase. The error bounds are calculated from the density bounds for the three observations. As is evident from the figure, the modeled intensity fails to reconcile with the observed intensity at higher altitudes. The discrepancy increases with altitude and is larger than the uncertainty in the data values. We attribute this difference in intensity to the presence of non-thermal H atoms, which was not accounted for in the modeling process.

4. Non-Thermal Hydrogen in the Martian Exosphere

Many attempts have been made in the past to understand the major processes that produce non-thermal H at Mars. An earlier study that focused on the production of hot H via exothermic reactions derived a hot to cold density ratio of $\sim 10^{-4}$ for low solar activity at the exobase (Lichtenegger et al., 2006; Nagy et al., 1990). This density of hot H is much too small to explain the discrepancy between the model and the HST data. A similar result was obtained for the production of hot H via photochemical reactions at Mars (Gregory et al., 2023; Gröller et al., 2015). A separate study dedicated toward understanding the production of hot H from collisions between thermal H and non-thermal O also predicted small ratios of energetic to thermal H densities (Shematovich, 2013), thereby disfavoring this mechanism as well. By contrast, the efficiency of the solar wind charge exchange process with exospheric thermal H and the resulting non-thermal H atoms created via secondary collisions (Bisikalo et al., 2018; Shematovich, 2013, 2021; Shematovich & Bisikalo, 2020, 2021) does appear to provide the needed number of hot atoms to explain the HST observations (exobase density ratio of hot to cold $\sim 10^{-3}$). Hence, for this study, we have focused on the third mechanism, the creation of non-thermal H through charge exchange with solar wind protons at Mars.

The non-thermal H density distribution at Mars is determined through 1D Monte Carlo (MC) modeling (Bisikalo et al., 2018; Shematovich, 2013, 2021; Shematovich & Bisikalo, 2020, 2021). The 1D model does not incorporate the increase in the volume of each voxel with altitude appropriate for spherical geometry, which may overestimate the number of non-thermal atoms by a factor $(r/R_{Mars})^2$. Including this change in volume may also result in the overproduction of energetic neutral H atoms from the solar wind charge exchange process, which then collide with thermal H to create non-thermal H atoms. The exact balance of the two factors and their effect on the true shape of the non-thermal H distribution profile is unknown at present. Such an undertaking requires extensive modeling and is beyond the scope of this study. However, the conclusion of this study is not expected to change significantly due to this modeling deficiency.

There are several inputs to the model: the thermal H density determined from the initial RT modeling of the data (Table 1), the upstream solar wind proton flux measured using the MAVEN Solar Wind Ion Analyzer instrument and displayed in Figure 3a, the temperature profile determined from the analytical expression of Krasnopolsky (2010), and the background atmospheric density for the major species CO_2 , N_2 , and O at Mars. The background temperature and density for the HST observations are displayed in Figure 3b.

The density of the background species was determined using the NGIMS instrument on MAVEN in conjunction with an atmospheric model (Matta et al., 2013; Mayyasi et al., 2019). The NGIMS observations were of CO_2 and Ar conducted on 17 December 2017, the closest date to the HST observations where the MAVEN periapsis was on the dayside allowing better constraints on the background atmosphere at low SZA. The background atmosphere was assumed to be unchanging for the period of the HST measurements. Even though this assumption is likely incorrect, specifically with regards to the scale height of the atmosphere due to the varying temperature profile, this effect was neglected in the analysis since no measurements exist for the HST observations. Also, the effect of the bulk atmospheric constituent and the primary Lyman α absorber, CO_2 , at Mars, is less than 1% above altitudes of 2,000 km (Chaufray et al., 2008).

The final-derived density of non-thermal H atoms from MC modeling is displayed in Figures 3c–3e. The calculated profiles indicate that non-thermal H is a significant constituent of the total H population at altitudes above 20,000 km for the three HST observations.

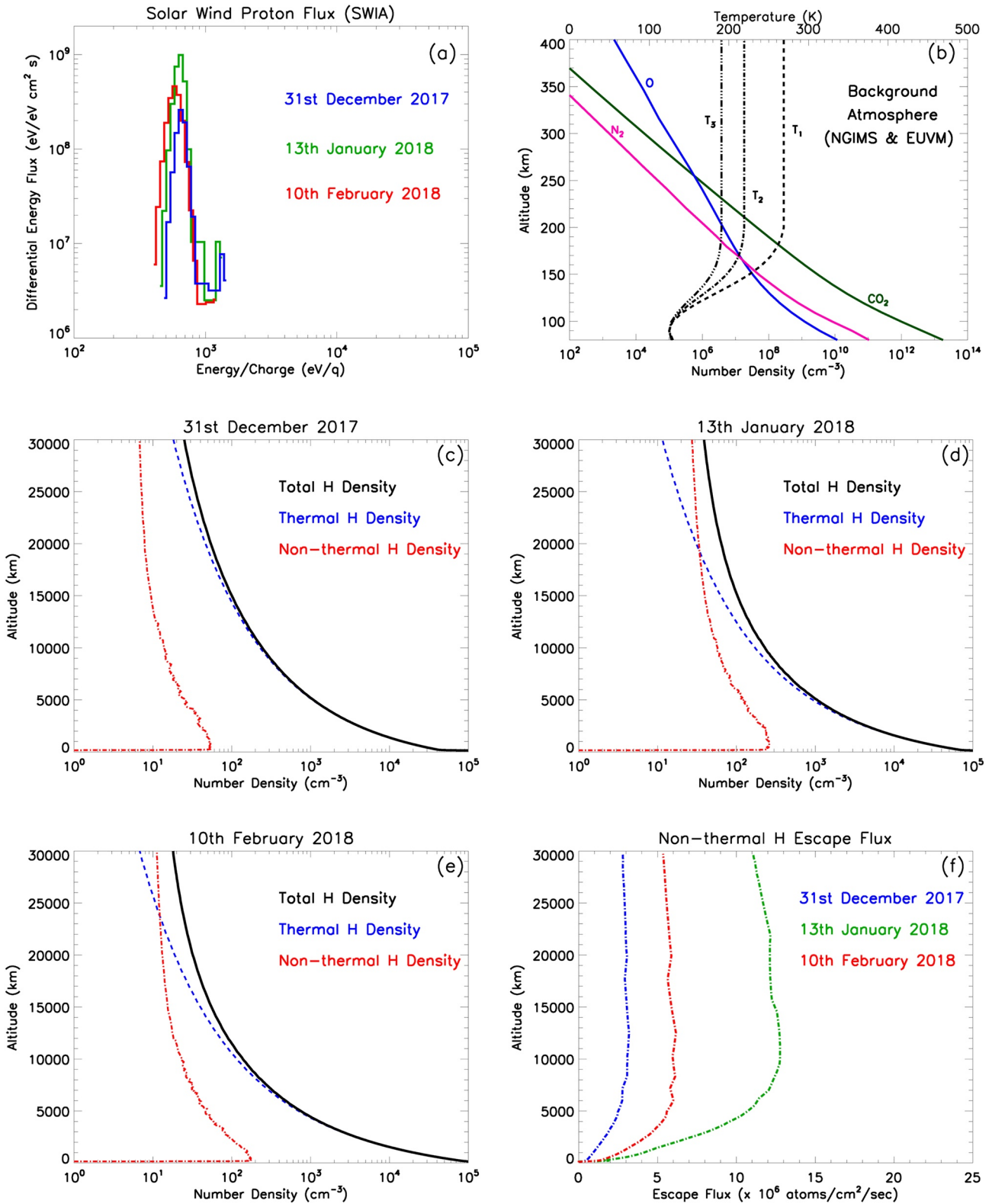


Figure 3.

The energetic and thermal H densities were then used in the RT model to simulate the observed intensity and compared with the data. For the RT simulation, the thermal and non-thermal populations were considered to not radiatively interact with each other. The RT model operates on the assumption that all H atoms obey the Maxwell Boltzmann (MB) velocity distribution at the exobase (Thomas, 1963). Since the hot H atoms were created via a non-thermal process and do not obey the MB distribution shape, a best-fit MB function of ~ 600 K was substituted in the RT model to represent them, as shown in Figure 2d. The resulting total intensity from the RT model successfully resolved the large discrepancy between the data and the model (Figure 2b). However, this modeled intensity was still below the observed value above 10,000 km. A second attempt at including the high energy tail of the non-thermal distribution fitted with a 10,000 K Maxwellian lowered the difference between data and model by 6% at higher altitudes (Figure 2c). This indicates that the higher energy atoms mostly reside at the largest altitudes, further confirming that the registered signal at altitudes $>20,000$ km is mostly from non-thermal H. Any leftover discrepancy is attributed to modeling shortcomings like not treating the non-thermal population accurately in the RT model, that is, assuming a photon redistribution function for a Maxwellian for the scattering process even though the actual velocity distribution of the particles is not Maxwellian, neglecting the contribution from other non-thermal processes, specifically HCO^+ dissociative recombination (Gregory et al., 2023), and inaccurate background atmospheric characteristics.

The escape rate of non-thermal atoms is determined from the MC model, which tracks the trajectories of the individual particles as a function of time. These escape rates with altitude are shown in Figure 3f. The Jeans escape formulation cannot be applied to this population as they do not obey the Maxwellian distribution. The mean escape rate for these hot atoms (calculated from the values in Figure 3f) from all altitudes amounted to $\sim 2.4 \times 10^6$, $\sim 9.9 \times 10^6$, and $\sim 4.9 \times 10^6$ atoms/cm²/s for 31 December 2017, 13 January 2018, and 10 February 2018, respectively. These escape rates when compared to the thermal rate (Table 1) indicate that the non-thermal escape fraction reached as high as $\sim 26\%$ of the thermal escape fraction from Mars under low solar activity conditions and colder thermospheric temperatures for the Martian atmosphere relative to those around perihelion.

Among the three HST visits, the upstream solar wind proton flux was highest on 13 January 2018. The altitude at which non-thermal H density exceeds the thermal H density ($\sim 20,000$ km) is also lowest on 13 January 2018. The 31 December 2017 date had the lowest upstream solar wind proton flux and the non-thermal H dominated altitudes were above 30,000 km and outside the field of view of HST. The exobase temperature was also the highest for that day, resulting in the largest scale height for thermal H among the three visits. This suggests that both the properties of thermal H, that is, its exobase density and temperature, and the upstream solar wind proton flux at Mars are contributing factors toward determining both the changeover altitude above which non-thermal H dominates and the escape flux of the non-thermal atoms from Mars.

5. Discussion

Determination of the actual amount of water lost by Mars has been a longstanding issue as has been mitigating the discrepancies between the surface D/H GEL value and the remote sensing GEL value. Discovery of an energetic H population in the Martian exosphere is a step in the right direction for resolving the GEL discrepancy and gaining a better understanding of the total water lost by Mars. The presence of this population also has significant impact on the exospheric dynamics (e.g., non-Maxwellian atoms change the velocity distribution and thereby shape of the emission line with altitude) of Mars and will likely shorten the timeline of the water escape history of the planet.

Hot H is present in the exospheres of all terrestrial planets in our solar system (Bhattacharyya et al., 2015; Chaufray et al., 2012; Qin & Waldrop, 2016). However, not much is known about the origin of this energetic population at present at all planets. At Mars, we find that the solar wind charge exchange is a viable mechanism for the creation of this population and could be a potential driver for other planets as well. Increased solar activity

Figure 3. Panel (a) shows the Mars Atmosphere and Volatile Evolution (MAVEN)-Solar Wind Ion Analyzer measurement of the solar wind proton flux at Mars for the three Hubble Space Telescope (HST) observation days. Panel (b) shows the background atmosphere constructed from MAVEN's Extreme UltraViolet Monitor and Neutral Gas and Ion Mass Spectrometer (NGIMS) instruments used in the modeling process. The T_1 (dashed curve), T_2 (dot-dash curve), and T_3 (dot-dot-dot-dash curve) correspond to the atmospheric temperatures for 31 December 2017, 13 January 2018, and 10 February 2018. The O, CO₂, and N₂ densities were determined from NGIMS measurements on 17 December 2017. Panels (c–e) show the thermal H density distribution obtained from radiative transfer modeling and the non-thermal H density distribution determined from the Monte Carlo (MC) model for the three HST observation days. The black line in the three figures represents the sum of the thermal and the non-thermal H densities. Panel (f) represents the non-thermal H escape flux calculated from the MC model as a function of altitude.

would therefore have a significant impact on the H escape rate at Mars and so would the injection of more H atoms above the exobase. Further study of this population has to be conducted during Mars' perihelion season, which is also the dust storm season ($L_s = 180^\circ\text{--}330^\circ$), when both the thermal H density and the upstream solar flux are higher. Because non-thermal H is created by energization of thermal H through collisions with the energetic neutral H atoms generated from charge exchange with the solar wind, as shown in this work, it is expected that the non-thermal escape rate would be higher during the perihelion season, thereby increasing the water escape rate during a Mars year.

In the past, when the Sun was younger and more active, the solar wind charge exchange rate with the neutral exospheric H atoms was likely higher, resulting in enhanced water escape for the planet. This implies that Mars could have probably lost most of its water early in its evolution, and the amount that remains buried in the crust today (100–1,500 m GEL) found from geological studies (Carr & Head, 2003; Clifford & Parker, 2001; Di Achille & Hynek, 2010; Korokawa et al., 2014) is likely closer to the lower end of the estimate. Therefore, elucidating the behavior of the energetic H atoms is key to extrapolating back in time to understand the history of water escape from the red planet as well as the possibility of the existence of life on it.

Data Availability Statement

The HST data used in this analysis can be found in the HST MAST archive through the link https://mast.stsci.edu/search/ui/#/hst/results?proposal_id=15097. The MAVEN data used in this study are publicly available through the NASA Planetary Data System (PDS) archive's Atmospheres node at https://pds-atmospheres.nmsu.edu/data_and_services/atmospheres_data/MAVEN/maven_main.html. The radiative transfer model source functions are available in Bhattacharyya et al. (2023a). The data presented in the figures are available in Bhattacharyya et al. (2023b).

Acknowledgments

The corresponding author thanks Luke Moore and Robert Johnson for their helpful insights into modeling the non-thermal H population at Mars. This research work was supported by the Space Telescope Science Institute (STScI) Grants GO-15097 to Boston University and GO-15595 to University of Illinois at Urbana-Champaign (UIUC). The research was also funded, in part, by NASA Contract 1000320450 from the University of Colorado to Boston University and by NASA Grant 80NSSC18K0266. JYC thanks CNES and the Programme National de Planétologie et Programme National Soleil-Terre for their support. V. S. and D. Bisikalo acknowledge the financial support of the RSCF Grant 22-12-00364.

References

- Anderson, D. E. (1976). The Mariner 5 ultraviolet photometer experiment – Analysis of hydrogen Lyman alpha data. *Journal of Geophysical Research*, *81*(7), 1213–1216. <https://doi.org/10.1029/ja081i007p01213>
- Baker, V. R. (2001). Water and the Martian landscape. *Nature*, *412*(6843), 228–236. <https://doi.org/10.1038/35084172>
- Barth, C. A., Fastie, W. G., Hord, C. W., Pearce, J. B., Kelly, K. K., Stewart, A. I., et al. (1969). Mariner 6 ultraviolet spectrum of Mars upper atmosphere. *Science*, *165*(3897), 1004–1005. <https://doi.org/10.1126/science.165.3897.1004>
- Barth, C. A., Pearce, J. B., Kelly, K. K., Anderson, G. P., & Stewart, I. A. (1971). Mariner 6 and 7 ultraviolet spectrometer experiment: Upper atmosphere data. *Journal of Geophysical Research*, *76*(10), 2213–2227. <https://doi.org/10.1029/ja076i10p02213>
- Bertaux, J.-L., Blamont, J., Marcelin, M., Kurt, V., Romanova, N., & Smirnov, A. (1978). Lyman-alpha observations of Venera 9 and 10. The non-thermal hydrogen population in the exosphere of Venus. *Planetary and Space Science*, *26*(9), 817–832. [https://doi.org/10.1016/0032-0633\(78\)90105-8](https://doi.org/10.1016/0032-0633(78)90105-8)
- Bhattacharyya, D., Chaufray, J., Mayyasi, M., Clarke, J., Stone, S., Yelle, R., et al. (2020). Two-dimensional model for the Martian exosphere: Applications to hydrogen and deuterium Lyman alpha observations. *Icarus*, *339*, 113573. <https://doi.org/10.1016/j.icarus.2019.113573>
- Bhattacharyya, D., Clarke, J., Mayyasi, M., Shematovich, V., Bisikalo, D., Chaufray, J.-Y., et al. (2023a). Mars thermal+non-thermal H modeling (V-1.0) [Software]. Zenodo. <https://doi.org/10.5281/zenodo.8002376>
- Bhattacharyya, D., Clarke, J., Mayyasi, M., Shematovich, V., Bisikalo, D., Chaufray, J.-Y., et al. (2023b). Mars thermal+non-thermal modeling data from figures (V-1.0) [Dataset]. Zenodo. Retrieved from <https://zenodo.org/record/8176255>
- Bhattacharyya, D., Clarke, J. T., Bertaux, J.-L., Chaufray, J.-Y., & Mayyasi, M. (2015). A strong seasonal dependence in the Martian hydrogen exosphere. *Geophysical Research Letters*, *42*(20), 8678–8685. <https://doi.org/10.1002/2015gl065804>
- Bhattacharyya, D., Clarke, J. T., Bertaux, J.-L., Chaufray, J.-Y., & Mayyasi, M. (2017a). Analysis and modeling of remote observations of the Martian hydrogen exosphere. *Icarus*, *281*, 264–280. <https://doi.org/10.1016/j.icarus.2016.08.034>
- Bhattacharyya, D., Clarke, J. T., Chaufray, J.-Y., Mayyasi, M., Bertaux, J.-L., Chaffin, M. S., et al. (2017b). Seasonal changes in hydrogen escape from Mars through analysis of HST observations of the Martian exosphere near perihelion. *Journal of Geophysical Research: Space Physics*, *122*(11), 11756–11764. <https://doi.org/10.1002/2017ja024572>
- Bisikalo, D. V., Shematovich, V. I., Gerard, J.-C., & Hubert, B. (2018). Monte Carlo Simulations of the interaction of fast proton and hydrogen atoms with the Martian atmosphere and comparison with in situ measurements. *Journal of Geophysical Research: Space Physics*, *123*(7), 5850–5861. <https://doi.org/10.1029/2018ja025400>
- Bougher, S., & Keating, G. M. (1999). Structure of the Mars upper atmosphere: MGS aerobraking data and model interpretation. In *The fifth international conference on Mars*. 1999 ficm conf.6010B.
- Bougher, S., McDunn, T. M., Zoldak, K. A., & Forbes, J. M. (2009). Solar cycle variability of Mars dayside exospheric temperatures: Model evaluation of underlying thermal balances. *Geophysical Research Letters*, *36*(5), L05201. <https://doi.org/10.1029/2008GL036376>
- Carr, M. H., & Head, J. W. (2003). Oceans on Mars: An assessment of the observational evidence and possible fate. *Journal of Geophysical Research*, *108*(E5), 5042. <https://doi.org/10.1029/2002je001963>
- Chaffin, M. S., Chaufray, J. Y., Deighan, J., Schneider, N. M., Mayyasi, M., Clarke, J. T., et al. (2018). Mars H escape rates derived from MAVEN/IUVS Lyman alpha brightness measurements and their dependence on model assumptions. *Journal of Geophysical Research: Planets*, *123*(8), 2192–2210. <https://doi.org/10.1029/2018je005574>

- Chaffin, M. S., Chaufray, J.-Y., Stewart, I., Montmessin, F., Schneider, N. M., & Bertaux, J.-L. (2014). Unexpected variability of Martian hydrogen escape. *Geophysical Research Letters*, *41*(2), 314–320. <https://doi.org/10.1002/2013gl058578>
- Chaufray, J.-Y., Bertaux, J.-L., LeBlanc, F., & Quemerais, E. (2008). Observation of the hydrogen corona with SPICAM on Mars express. *Icarus*, *195*(2), 598–613. <https://doi.org/10.1016/j.icarus.2008.01.009>
- Chaufray, J.-Y., Bertaux, J.-L., Quemerais, E., Villard, E., & Leblanc, F. (2012). Hydrogen density in the dayside Venusian exosphere derived from Lyman-alpha observations by SPICAV on Venus Express. *Icarus*, *217*(2), 767–778. <https://doi.org/10.1016/j.icarus.2011.09.027>
- Clarke, J. T., Bertaux, J.-L., Chaufray, J.-Y., Gladstone, G., Quemerais, E., Wilson, J., & Bhattacharyya, D. (2014). A rapid decrease of the hydrogen corona of Mars. *Geophysical Research Letters*, *41*(22), 8013–8020. <https://doi.org/10.1002/2014gl061803>
- Clarke, J. T., Mayyasi, M., Bhattacharyya, D., Schneider, N. M., McClintock, W. E., Deighan, J. I., et al. (2017). Variability of D and H in the Martian upper atmosphere observed with the MAVEN IUVS echelle channel. *Journal of Geophysical Research: Space Physics*, *122*(2), 2336–2344. <https://doi.org/10.1002/2016ja023479>
- Clarke, J. T., Nichols, J., Gérard, J. C., Grodent, D., Hansen, K. C., Kurth, W., et al. (2009). Response of Jupiter's and Saturn's auroral activity to the solar wind. *Journal of Geophysical Research*, *114*(A5), A05210. <https://doi.org/10.1029/2008JA013694>
- Clifford, S. M., & Parker, T. J. (2001). The evolution of the Martian hydrosphere: Implications for the fate of a primordial ocean and the current state of the northern plains. *Icarus*, *154*(1), 40–79. <https://doi.org/10.1006/icar.2001.6671>
- Di Achille, G., & Hynek, B. M. (2010). Ancient ocean on Mars supported by global distribution of deltas and valleys. *Nature Geoscience*, *3*(7), 459–463. <https://doi.org/10.1038/ngeo891>
- Ehlmann, B. L., Mustard, J. F., Murchie, S. L., Bibring, J. P., Meunier, A., Fraeman, A. A., & Langevin, Y. (2011). Subsurface water and clay mineral formation during the early history of Mars. *Nature*, *479*(7371), 53–60. <https://doi.org/10.1038/nature10582>
- Forget, F., Hourdin, F., Fournier, R., Hourdin, C., Talagrand, O., Collins, M., et al. (1999). Improved general circulation models of the Martian atmosphere from the surface to above 80 km. *Journal of Geophysical Research*, *24*(E10), 155–175. <https://doi.org/10.1029/1999je001025>
- Gonzalez-Galindo, F., Forget, F., Lopez-Valverde, M. A., Angelats I Coll, M., & Millour, E. (2009). A ground-to-exosphere general circulation model: 1. Seasonal, diurnal, and solar cycle variation of thermospheric temperatures. *Journal of Geophysical Research*, *114*(E4), E04001. <https://doi.org/10.1029/2008je003246>
- Gregory, B. S., Elliott, R. D., Deighan, J., Gröller, H., & Chaffin, M. S. (2023). HCO⁺ dissociative recombination: A significant driver of nonthermal hydrogen loss at Mars. *Journal of Geophysical Research: Planets*, *128*(1), e2022JE007576. <https://doi.org/10.1029/2022je007576>
- Gröller, H., Lichtenegger, H., Lammer, H., & Shematovich, V. I. (2015). Hydrogen coronae around Mars and Venus. *EPSC Abstracts*, *10*. EPSC2015-397.
- Halekas, J. S. (2017). Seasonal variability of the hydrogen exosphere of Mars. *Journal of Geophysical Research: Planets*, *122*(5), 901–911. <https://doi.org/10.1002/2017je005306>
- Hunten, D. M., & McElroy, M. B. (1970). Production and escape of hydrogen on Mars. *Journal of Geophysical Research*, *75*(31), 5589–6001. <https://doi.org/10.1029/ja075i031p05989>
- Jakosky, B. M., Brain, D., Chaffin, M., Curry, S., Deighan, J., Grebowsky, J., et al. (2018). Loss of the Martian atmosphere to space: Present-day loss rates determined from MAVEN observations and integrated loss through time. *Icarus*, *315*, 146–157. <https://doi.org/10.1016/j.icarus.2018.05.030>
- Jakosky, B. M., & Philips, R. J. (2001). Mars' volatile and climate history. *Nature*, *412*(6843), 237–244. <https://doi.org/10.1038/35084184>
- Korokawa, H., Sato, M., Ushioda, M., Matsuyama, T., Moriwaki, R., Dohm, J. M., & Usui, T. (2014). Evolution of water reservoirs on Mars: Constraints from hydrogen isotopes in Martian meteorites. *Earth and Planetary Science Letters*, *394*, 179–185. <https://doi.org/10.1016/j.epsl.2014.03.027>
- Krasnopolsky, V. A. (2010). Solar activity variations of thermospheric temperatures on Mars and a problem of CO in the lower atmosphere. *Icarus*, *207*(2), 638–647. <https://doi.org/10.1016/j.icarus.2009.12.036>
- Leblanc, F., Chaufray, J.-Y., & Bertaux, J.-L. (2007). On Martian nitrogen dayglow emission observed by SPICAM UV spectrograph/Mars Express. *Geophysical Research Letters*, *34*(2), L02206. <https://doi.org/10.1029/2006gl028437>
- Leblanc, F., Chaufray, J.-Y., Witasse, O., Liliensten, J., & Bertaux, J.-L. (2006). The Martian dayglow as seen by SPICAM UV spectrometer on Mars Express. *Journal of Geophysical Research*, *111*(E9), E09S11. <https://doi.org/10.1029/2005je002664>
- Lichtenegger, H. I. M., Lammer, H., Kulikov, Y. N., Kazeminejad, S., Molina-Cuberos, G. H., Rodrigo, R., et al. (2006). Effects of low energetic neutral atoms to Martian and Venusian exospheric temperature estimations. *Space Science Reviews*, *126*(1–4), 469–501. <https://doi.org/10.1007/s11214-006-9082-1>
- Matta, M., Withers, P., & Mendillo, M. (2013). The composition of Mars' topside ionosphere: Effects of hydrogen. *Journal of Geophysical Research: Space Physics*, *118*(5), 2681–2693. <https://doi.org/10.1002/jgra.50104>
- Mayyasi, M., Bhattacharyya, D., Clarke, J., Catalano, A., Benna, M., Mahaffy, P., et al. (2018). Significant space weather impact on the escape of hydrogen from Mars. *Geophysical Research Letters*, *45*(17), 8844–8852. <https://doi.org/10.1029/2018gl077727>
- Mayyasi, M., Clarke, J., Bhattacharyya, D., Chaufray, J. Y., Benna, M., Mahaffy, P., et al. (2019). Seasonal variability of deuterium in the upper atmosphere of Mars. *Journal of Geophysical Research: Space Physics*, *124*(3), 2152–2164. <https://doi.org/10.1029/2018ja026244>
- Mayyasi, M., Clarke, J., Chaufray, J. Y., Kass, D., Bougher, S., Bhattacharyya, D., et al. (2022). Solar cycle and seasonal variability of H in the upper atmosphere of Mars. *Icarus*, *393*, 115293. <https://doi.org/10.1016/j.icarus.2022.115293>
- McElroy, M. B., & Donahue, T. M. (1972). Stability of the Martian atmosphere. *Science*, *177*(4053), 986–988. <https://doi.org/10.1126/science.177.4053.986>
- Nagy, A., Kim, J., & Cravens, T. E. (1990). Hot hydrogen and oxygen in the upper atmospheres of Venus and Mars. *Annales Geophysicae*, *8*, 251–256.
- Ojha, L., Wilhelm, M. B., Murchie, S. L., McEwen, A. S., Wray, J. J., Hanley, J., et al. (2015). Spectral evidence for hydrated salts in recurring slope lineae on Mars. *Nature Geoscience*, *8*(11), 829–832. <https://doi.org/10.1038/ngeo2546>
- Parkinson, T. D., & Hunten, D. M. (1972). Spectroscopy and acronomy of O₂ on Mars. *Journal of the Atmospheric Sciences*, *29*(7), 1380–1390. [https://doi.org/10.1175/1520-0469\(1972\)029<1380:saoo>2.0.co;2](https://doi.org/10.1175/1520-0469(1972)029<1380:saoo>2.0.co;2)
- Qin, J., & Waldrop, L. (2016). Non-thermal hydrogen atoms in the terrestrial upper thermosphere. *Nature Communications*, *7*(1), 13655. <https://doi.org/10.1038/ncomms13655>
- Ryon, J. E. et al. (2023). “ACS instrument handbook,” version 22.0 (Baltimore: STScI).
- Shematovich, V. I. (2013). Suprathermal oxygen and hydrogen atoms in the upper Martian atmosphere. *Solar System Research*, *47*(6), 437–445. <https://doi.org/10.1134/s0038094613060087>
- Shematovich, V. I. (2021). Atmospheric loss of atomic oxygen during proton aurorae on Mars. *Solar System Research*, *55*(4), 322–332. <https://doi.org/10.1134/s0038094621040079>

- Shematovich, V. I., & Bisikalo, D. V. (2020). Kinetic calculations of the charge exchange efficiency between solar wind protons and extended hydrogen corona of Mars. *Astronomy Reports*, *64*(10), 863–869. <https://doi.org/10.1134/s1063772920110074>
- Shematovich, V. I., & Bisikalo, D. V. (2021). A kinetic model for precipitation of solar wind protons into the Martian atmosphere. *Astronomy Reports*, *65*(9), 869–875. <https://doi.org/10.1134/s106377292110036x>
- Stone, S., Yelle, R. V., Benna, M., Elrod, M., & Mahaffy, P. (2018). Thermal structure of the Martian upper atmosphere from MAVEN NGIMS. *Journal of Geophysical Research: Planets*, *123*(11), 2842–2867. <https://doi.org/10.1029/2018je005559>
- Thiemann, E. M. B., Eparvier, F. G., Bougher, S. W., Dominique, M., Andersson, L., Girazian, Z., et al. (2018). Mars thermospheric variability revealed by MAVEN EUVM solar occultations: Structure at aphelion and perihelion and response to EUV forcing. *Journal of Geophysical Research: Planets*, *123*(9), 2248–2269. <https://doi.org/10.1029/2018je005550>
- Thomas, G. E. (1963). Lyman alpha scattering in the Earth's hydrogen geocorona 1. *Journal of Geophysical Research*, *68*(9), 2639–2660. <https://doi.org/10.1029/jz068i009p02639>
- Villanueva, G., Mumma, M. J., Novak, R. E., Käufel, H. U., Hartogh, P., Encrenaz, T., et al. (2015). Strong water isotopic anomalies in the Martian atmosphere: Probing current and ancient reservoirs. *Science*, *348*(6231), 218–221. <https://doi.org/10.1126/science.aaa3630>
- Waldrop, L., & Paxton, L. (2013). Lyman α airglow emission: Implications for atomic hydrogen geocorona variability with solar cycle. *Journal of Geophysical Research: Space Physics*, *118*(9), 5874–5890. <https://doi.org/10.1002/jgra.50496>